Mass and radius constraints of neutron stars from pulse shape modelling

Master Thesis
University of Turku
Department of Physics and Astronomy
Astronomy
2016
Tuomo Salmi
Supervised by:
J.P.
J.N.

University of Turku
Department of Physics and Astronomy

Salmi, Tuomo Mass and radius constraints of neutron stars from pulse shape modelling

Master's thesis, 19 s., 3 Appendices
Astronomy
September 2016

Write here!

Contents

Introduction

Rapidly rotating neutron stars, called pulsars, are the lighthouses of the universe. Pulses can be observed when an electromagnetic beam from the neutron star is emitted towards the Earth. This emission is thought be created when matter is accreted to a hot spot on a magnetic pole at the surface of the pulsar. These pulses or light curves can be detected in many wavelengths. For example the most rapidly rotating pulsars, called millisecond pulsars, have been detected in the radio, X-ray, and gamma ray portions of the electromagnetic spectrum.

The exact shape of the pulses may reveal us important information about the properties of the neutron stars. The determination of the mass-radius relation of neutron stars through observations is one of the fundamental problems in neutron star astrophysics. This information could provide tight constraints on the equation of state of ultra-dense matter located inside the neutron star. This high densities of cold matter is otherwise unattainable. Studies of the light curves of pulsars can therefore help determine the properties of such matter. It is also not overstated to say that the properties of matter at extremely high densities are also among the most important questions in physics and astronomy.

One way to constrain masses and radii is to use X-ray burst observations of neutron stars. Models of burst oscillations waveforms (pulses during the burst) can be fit to observations of these waveforms. The mass and radius of neutron star have an effect to the waveform because of the influence e.g. on the light bending due to general relativity. However many other parameters have also an impact on the light curves making it challenging to get tight constraints to radius and mass. Markov chain Monte Carlo sampling and high-performance computing are necessities when trying to find correct values for these parameters.

1 Neutron stars

Neutron stars are some of the densest and most massive objects in the universe. Typical mass of a neutron star (M) is on the order of 1.5 solar masses ($M_{\odot}$), and typical radius R on the order of 12 km. The central density n_c can be from 5 to 10 times the nuclear equilibrium density $n_0 \approx 0.16 fm^{-3}$ of neutrons and protons found in laboratory nuclei [1]. Neutrons dominate the nucleonic component of neutron stars, but also some protons, electrons and muons exist. At the supernuclear densities also more exotic baryons, mesons or quarks may appear.

Neutron stars are created after the gravitational collapse of the core of a massive star (>8$M_{\odot}$) at the end of its life, which triggers a Type II supernova explosion. Too massive stars collapse instead into a black hole. The general relativistic Schwarzschild condition

$$R > \frac{2GM}{c^2}, \tag{1}$$

where G is the gravitational constant and c is the speed of light, constrains the possible mass and radius of neutron stars.

A more strict upper bound to the compactness (ratio between mass and radius) of the star follows the fact [2] that the speed of sound in dense matter have to be less than the speed of light. This gives us the so called causality condition

$$R \gtrsim \frac{3GM}{c^2}. \tag{2}$$

Neutron stars have also a minimum stable neutron star mass, which is about 0.1 $M_{\odot}$, although the neutron star's origin in a supernova gives a more realistic minimum [1].

Generally the mass-radius (M-R) relation, is determined by the equations of hydrostatic equilibrium. For a spherical object under hydrostatic equilibrium in general relativity these are the the so called Tolman-Oppenheimer-Volkov equations (Tolman, 1934; Oppenheimer & Volkoff, 1939):

$$\frac{dP}{dr} = -\frac{G[m(r) + 4\pi r^3 P/c^2](\rho + P/c^2)}{r[r - 2Gm(r)/c^2]}, \tag{3}$$

and

$$\frac{dm(r)}{dr} = 4\pi\rho r^2, \tag{4}$$

where P and ρ are the pressure and mass-energy density, respectively, and m(r) is the gravitational mass enclosed within a radius r. M-R relation can now be obtained if the relation between pressure and density $P = P(\rho)$ is known. The relation we call the equation of state (EOS). For a realistic EOS the previous equations must be numerically solved to obtain M-R relation. These can be separated into three categories according to the compressibility of the matter: soft, moderate and stiff equations of state.

One more potential constraint on the EOS is based on the rotation of neutron stars. The velocity of the stellar surface cannot exceed the velocity of an orbiting particle suspended just above the surface ("break-up frequency"). The highest observed spin rate gives a lower limit to the compactness of the neutron star.

1.1 Accreting millisecond pulsars

Since the discovery of neutron stars as radio pulsars in 1967, many different classes have been discovered including low mass X-ray binaries (LMXBs). In LMXBs the neutron star accretes matter from a non-collapsed stellar companion (with mass M $\gtrsim M_\odot$) via an accretion disk. Accreting millisecond X-ray pulsars (AMXPs) is a subgroup of the LMXBs, in which the gas stripped from the companion is channeled out of the accretion disk onto the magnetic poles of the rotating neutron star. This gives rise to the X-ray pulsations at the spin frequency of the neutron star. By definition AMXPs are also spinning at frequencies $\nu \geq 100\,\mathrm{Hz}$ and have weak surface magnetic fieds ($B \sim 10^{8-9}$) [3]. All known AMXPs have donor stars that transfer mass via Roche lobe overflow.

The first AMXP discovered was SAX J1808.4–3658. It is also the main observed target in this thesis. The source was first found in 1996 by the Italian-Dutch BeppoSAX satellite, but the first coherent pulsations (at 401 Hz) were detected during the second outburst with Rossi X-ray Timing Explorer (RXTE) in 1998. It provided a confirmation of the "recycling scenario", wchich states that AMXPs are the evolutionary progenitors of recycled radio millisecond pulsars. They are responsible for the conversion of slow neutron stars with high magnetic field ($B \sim 10^{12}$), into a rapidly spinning objects with a relatively weak magnetic field ($B \sim 10^{8}$) [3].

SAX J1808.4–3658 went into outburst again in 2000, 2002, 2005, 2008 and 2011, with an approximate recurrence time of about 1.6-3.3 yr, and is the best sampled and studied of all AMXPs. The typical outburst can be split in five phases: a fast rise, with a steep increase in luminosity lasting only a few days, a peak, a slow decay stage, a fast decay phase and the flaring tail. Except the last phase, they can in principle be partially explained with the disk instability model.

The X-ray spectrum of the outbursts have also been analysed and there is evidence for a two component-model: a blackbody at soft energies and a hard Comptonization component at higher energies [4] . The blackbody is interpreted as the heated hot spot on the neutron star surface and the Comptonization is produced in a accretion shock. This shock is created at the bottom of the magnetic field lines as the plasma abruptly decelerates close to the neutron star surface.

2 Methods

2.1 Pulse profile modelling

The oscillations in the flux during the outbursts (the light curves) of accreting millisecond pulsars (described in the first chapter) can be modelled with different models. The model presented here assumes that the radiation is originated from one or two polar spots locating at the polar caps of the stars. General and special relativistic effects have been taken account using so called Schwarzschild-Doppler (S+D) approximation (Miller, Lamb 1998, Poutanen, Gierlinski 2003) [5]. In the S+D approximation the gravitational light-bending effects are modelled as though the star is not rotating using the Schwarzschild metric and the formalism prescribed by Pechenick, Ftaclas and Cohen (1983) [6]. Rotational effects are added by introducing Doppler terms as though the star is a rotating object with no gravitational field. The oblate shape of the rapidly rotating neutron stars have also been taken account using an empirical formula for the oblate shape.

2.1.1 Oblateness

Due to the fast rotation the millisecond pulsars have an oblate shape instead of spherical. The difference between oblate and spherical star are significant when the rotation frequency $\nu \geq 300\,\mathrm{Hz}$. The most important effect is purely geometrical: The directions that the light can be emitted into are different in these two cases. Thus there are certain spot locations on the star where the spot is visible if the surface is oblate but would be invisible if the surface where spherical (and vice versa).

The exact shape and oblateness of the star (function $R(\theta)$) can be chosen from different models (θ is the colatitude measured from the spin axis). One of the most recent ones was presented by Algendy et. al. (2014) [7]. It is also the most used model in this thesis. In that model (in geometric units where G = c = 1)

$$\frac{R(\theta)}{R_{eq}} = (1 + o_2(x, \bar{\Omega})), \tag{5}$$

where

$$o_2(x, \bar{\Omega}) = \bar{\Omega}^2(-0.788 + 1.030x), \tag{6}$$

$$x = \frac{M}{R_{eq}}, \tag{7}$$

$$\bar{\Omega} = \Omega(\frac{R_{eq}^3}{M})^{1/2}. \quad (8)$$

In these equations R_{eq} is the radius of the rotating star measured at the equator and $\Omega = 2\pi/P$, where P is the spin period.

2.1.2 Geometry

We consider a small spot on the stellar surface at colatitude θ. The star is assumed to be rotating with frequency $\nu = P^{-1}$. The velocity of the spot in units of c is

$$x = \frac{v}{c} = \frac{2\pi R(\theta)}{c} \frac{\nu}{\sqrt{1-u}} \sin\theta = \beta_{\rm eq} \sin\theta, \quad (9)$$

where $\beta_{\rm eq}$ is the velocity at the equator (if $\theta = \frac{\pi}{2}$), $u \equiv r_{\rm S}/R(\theta)$, $r_{\rm S} = 2GM/c^2$ is the Schwarzschild radius, M is mass and R is radius of the star at spot location. The pulsar frequency has been corrected for the redshift $1/\sqrt{1-u} = 1+z$. The corresponding Lorentz factor is $\Gamma = (1-\beta^2)^{-1/2}$.

Spot area measured in the corotating frame is $\mathrm{d}S'$, and its instantaneous position in the fixed lab frame is described by the unit vector

$$\boldsymbol{r} = (\sin\theta\cos\phi, \sin\theta\sin\phi, \cos\theta), \quad (10)$$

that points to the spot from the star center (see Fig. 1). The rotational phase of the pulsar is $\phi = 2\pi\nu t$. The vector that points normal to the surface is

$$\boldsymbol{n} = (\sin(\theta-\gamma)\cos\phi, \sin(\theta-\gamma)\sin\phi, \cos(\theta-\gamma)). \quad (11)$$

The angle between $\boldsymbol{n}$ and $\boldsymbol{r}$ is γ and

$$\cos\gamma = [1 + f^2(\theta)]^{-1/2}, \quad (12)$$

where

$$f(\theta) = \frac{1+z}{R}\frac{dR}{d\theta}. \quad (13)$$

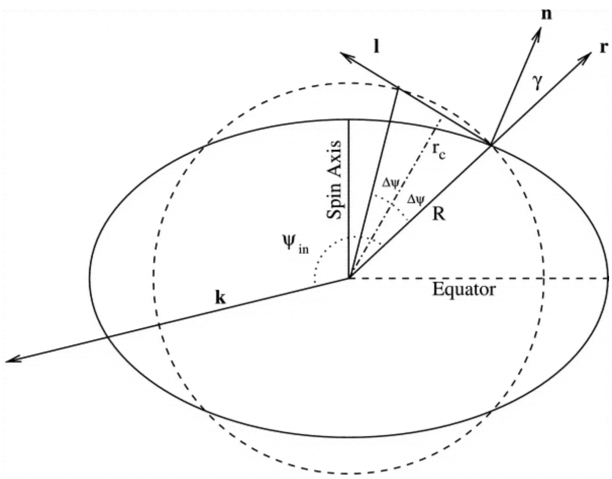

Fig. 1. Geometry of the problem. Dotted curve shows a spherical star which radius is equal to the radius of the oblate star at spot location ([8]).

We will start the waveform with the center of the spot in the plane defined by the spin axis and the direction to the observer (when the spot crosses the plane defined by $\boldsymbol{k}$ and $\boldsymbol{z}$). The light pulse originating at this moment at the point that is directly below the observer and with a reference distance to the center of the star (e.g. the equator radius of the star) is used to define the zero of the observer's time coordinate. The time is zero when this photon arrives at the observer.

We denote the unit vector along the line of sight by

$$\boldsymbol{k} = (\sin i, 0, \cos i), \tag{14}$$

where i is the inclination angle of the spin axis to the line of sight. Thus

$$\cos\psi = \boldsymbol{k} \cdot \boldsymbol{r} = \cos i \ \cos\theta + \sin i \ \sin\theta \ \cos\phi, \tag{15}$$

Angle ψ measures the apparent inclination of the spot to the line of sight, which is different from the true inclination because of the light bending effect. We denote the initial direction of the emitted photon by $\boldsymbol{k}_0$ ($\boldsymbol{l}$ in figure 1) and the true emission angle (relative to the radius vector) by α, so that

$$\cos\alpha = \boldsymbol{k}_0 \cdot \boldsymbol{r}. \tag{16}$$

The zenith angle σ between the $\boldsymbol{n}$ and $\boldsymbol{k_0}$ is defined by

$$\cos\sigma = \boldsymbol{k_0}\cdot\boldsymbol{n}. \tag{17}$$

As a photon propagates to infinity, its direction changes from $\boldsymbol{k}_0$ near the stellar surface to $\boldsymbol{k}$ at infinity, so that $\cos\alpha = \boldsymbol{k}_0\cdot\boldsymbol{r}$ changes to $\cos\psi = \boldsymbol{k}\cdot\boldsymbol{r}$. The relation between $\boldsymbol{k}_0$ and $\boldsymbol{k}$ may be written as

$$\boldsymbol{k}_0 = [\sin\alpha\,\boldsymbol{k} + \sin(\psi-\alpha)\,\boldsymbol{r}]/\sin\psi. \tag{18}$$

At any moment of time, we can introduce an instantaneous non-rotating frame x, y, z with the y-axis along the direction of the spot motion, x-axis along the meridian towards the equator, and z-axis along the normal to the spot. In this static frame

$$\boldsymbol{k}_0 = (\cos\epsilon, \cos\xi, \cos\sigma)\,, \tag{19}$$

where ξ is the angle between the spot velocity and $\boldsymbol{k}_0$:

$$\cos\xi = \frac{\boldsymbol{\beta}}{\beta}\cdot\boldsymbol{k}_0 = \frac{\sin\alpha}{\sin\psi}\frac{\boldsymbol{\beta}}{\beta}\cdot\boldsymbol{k} = -\frac{\sin\alpha}{\sin\psi}\sin i\ \sin\phi\,, \tag{20}$$

since $\boldsymbol{\beta} = \beta(-\sin\phi, \cos\phi, 0)$ in lab frame. And ϵ is the angle between the meridian

$$\boldsymbol{m} = (\cos(\theta-\gamma)\cos\phi, \cos(\theta-\gamma)\sin\phi, -\sin(\theta-\gamma)) \tag{21}$$

and $\boldsymbol{k}_0$:

$$\begin{aligned}\cos\epsilon = \boldsymbol{m}\cdot\boldsymbol{k}_0 = &\frac{\sin\alpha}{\sin\psi}(\sin i\cos(\theta-\gamma)\cos\phi - \cos i\sin(\theta-\gamma))\\ &+\frac{\sin(\psi-\alpha)}{\sin\psi}(\sin\theta\cos(\theta-\gamma) - \sin(\theta-\gamma)\cos\theta).\end{aligned} \tag{22}$$

Emission angle in the corotating frame relative to the surface normal is denoted by σ'. It differs from σ because of relativistic aberration. The rays of light are tilted towards the direction of the spot motion relative to the observer. In the frame comoving with the spot (with y-axis along the spot motion, z-axis along the local normal), the unit vector along the photon momentum is obtained from the Lorentz transformation:

$$\boldsymbol{k}_0' = \delta \begin{pmatrix} \cos\epsilon \\ \Gamma(\cos\xi - \beta) \\ \cos\sigma \end{pmatrix}, \tag{23}$$

where the Doppler factor

$$\delta = \frac{1}{\Gamma(1 - \beta\cos\xi)}. \tag{24}$$

Using equation (23), we obtain

$$\cos\sigma' = \delta\ \cos\sigma, \tag{25}$$

Making use of equation (18) the zenith angle has the value

$$\begin{gathered} \cos\sigma = \boldsymbol{k_0} \cdot \boldsymbol{n} = \cos\alpha\cos\gamma + \sin\alpha\sin\gamma\cos\delta = \\ \cos\alpha\cos\gamma + (\sin\alpha/\sin\psi)\sin\gamma(\cos i\sin\theta - \sin i\cos\theta\cos\phi), \end{gathered} \tag{26}$$

where the spherical trigonometric identity $\cos i = \cos\theta\cos\psi + \sin\theta\sin\psi\cos\delta$ (where δ is the angle between spot-observer and spot-spin-axis planes) and the equation (15) are used. With small bending angles the approximation $\sin\alpha/\sin\psi \approx \sqrt{(1-u)}$ is used.

2.1.3 Light bending

The exact relation between α and ψ (when $\alpha < \pi/2$) in Schwarzschild geometry (i.e. light bending) is given by (... [9])

$$\psi_p(R, \alpha) = \int_R^\infty \frac{dr}{r^2} \left[\frac{1}{b^2} - \frac{1}{r^2}\left(1 - \frac{r_S}{r}\right) \right]^{-1/2}, \tag{27}$$

where b is impact parameter,

$$b = \frac{R}{\sqrt{1-u}} \sin\alpha. \tag{28}$$

The maximum bending angle corresponds to $\sigma = \pi/2$. Otherwise the photon would be directed across the star surface. The visibility of the spot is thus defined by a condition

$\cos\sigma > 0$. In addition one should also check that the photon won't hit the surface of the star in any later phase of it's trajectory (it might be possible for an oblate star). This check is not yet included in the current pulse profile code.

The relation between α and ψ, when $\alpha > \pi/2$, is

$$\psi(R,\alpha) = 2\psi_{\max} - \psi_p(R, \pi - \alpha), \tag{29}$$

where $\psi_{\max} = \psi_p(p, \alpha = \pi/2)$ and p is the distance of closest approach, given by

$$p = -\frac{2}{\sqrt{3}} b \cos([arcos(3\sqrt{3} r_s/(2b)) + 2\pi]/3). \tag{30}$$

2.1.4 Observed flux

The observed flux from the spot at photon energy E is

$$\mathrm{d}F_E = I_E \, \mathrm{d}\Omega, \tag{31}$$

where I_E is the specific intensity of radiation at infinity and $\mathrm{d}\Omega$ is the solid angle occupied by spot with area $\mathrm{d}S'$ on the observer's sky. The solid angle can be expressed in terms of the impact parameter

$$\mathrm{d}\Omega = b \, \mathrm{d}b \, \mathrm{d}\varphi / D^2, \tag{32}$$

where D is the distance to the source and φ is the azimuthal angle corresponding to rotation around line of sight (vector $\boldsymbol{k}$). The impact parameter b depends on ψ only, but not on φ.

The apparent area of the spot as measured by photon beams in the non-rotating frame near the stellar surface is $\mathrm{d}S = \delta \, \mathrm{d}S'$ (see Terrell 1959; Lightman et al. 1975; Ghisellini 1999) and the relation between σ and σ' is described by the relativistic aberration formula (for motions parallel to the spot surface) (25). Thus the spot area projected on to the plane perpendicular to the photon propagation direction, i.e. a photon beam cross-section, is Lorentz invariant (see e.g. Lightman et al. 1975; Lind & Blandford 1985):

$$\mathrm{d}S \ \cos\sigma = \mathrm{d}S' \ \cos\sigma'. \tag{33}$$

Combining this information to equation derived by (...)the solid angle is

$$\mathrm{d}\Omega = \frac{\mathrm{d}S' \cos\sigma'}{D^2} \frac{1}{1-u} \frac{\mathrm{d}\cos\alpha}{\mathrm{d}\cos\psi}. \tag{34}$$

In the limit of weak gravity $u \ll 1$, this gives the usual formula $\mathrm{d}\Omega = \mathrm{d}S' \cos\sigma' / D^2$.

The combined effect of the gravitational redshift and Doppler effect results in the following relation between the monochromatic observed and local intensities (...)

$$I_E = \left(\frac{E}{E'} \right)^3 I'_{E'}(\sigma') \tag{35}$$

where $E/E' = \delta\sqrt{1-u}$. Here $I'_{E'}(\sigma')$ is the intensity computed in the frame comoving with the spot. For the bolometric intensity, one gets

$$I = \left(\delta\sqrt{1-u}\right)^4 I'(\sigma'). \tag{36}$$

The observed spectral flux (eq. 31) now reads

$$F_E = (1-u)^{1/2} \delta^4 I'_{E'}(\sigma') \cos\sigma \frac{\mathrm{d}\cos\alpha}{\mathrm{d}\cos\psi} \frac{\mathrm{d}S'}{D^2}, \tag{37}$$

where we have used the aberration formula (25). The bolometric flux is given by:

$$F = (1-u)\, \delta^5\, I'(\sigma') \cos\sigma \frac{\mathrm{d}\cos\alpha}{\mathrm{d}\cos\psi} \frac{\mathrm{d}S'}{D^2}. \tag{38}$$

If the radiation spectrum can be represented by a power-law $I'_{E'}(\sigma') \propto E'^{-(\Gamma-1)}$ with a photon spectral index Γ which does not depend on the angle σ' then

$$I'_{E'}(\sigma') = I'_E(\sigma') \left(\delta\sqrt{1-u}\right)^{\Gamma-1}. \tag{39}$$

The observed spectral flux at a distance D from the star is then given by

$$F_E = (1-u)^{\Gamma/2}\, \delta^{\Gamma+3} I'_E(\sigma') \cos\sigma\, \frac{\mathrm{d}\cos\alpha}{\mathrm{d}\cos\psi}\, \frac{\mathrm{d}S'}{D^2}. \tag{40}$$

Expression for the bolometric flux (38) may be obtained as a special case of Eq. (40) by setting $\Gamma = 2$.

Thus, the bolometric flux from a rapidly rotating star differs by a factor δ^5 from that for a slowly rotating star. Two powers of δ come from the solid angle transformation, one from the energy, one from the photon arrival time contraction, and the fifth from the change in the projected area due to aberration. Aberration may also change the specific intensity since it has to be computed for angle σ' in the comoving frame

2.1.5 Time delays

Expressions (37), (38) and (40) contain the pulsar phase ϕ, but the flux actually corresponds to a different observed phase $\phi_{\rm obs}$, which is different from ϕ due to light travel delays. The delays become significant only for rapidly rotating pulsars. In Schwarzschild metric the maximum time delay for a neutron star of $M = 1.4{\rm M}_{\odot}$ is $\Delta t \sim 7 \times 10^{-2}$ ms (almost independent of compactness of the star M/R). This gives at most a 5 per cent correction to the arrival phase for a rotational period $P = 1.5$ ms.

The delay is caused by different travel times of emitted photons to the observer, depending on the position of the emitting spot. A photon following the trajectory with an impact parameter b (and $\alpha < \pi/2$) is lagging the photon originating from a reference radius r_{ref} (which can be chosen arbitrarily as long as it exceeds $r_{\rm S}$) with $b = 0$ by (...):

$$c\Delta t_p(R,\alpha) = c\Delta t_s(R,\alpha) - \delta t(r_{ref}, R), \tag{41}$$

where

$$c\Delta t_s(R,\alpha) = \int_R^{\infty} \frac{{\rm d}r}{1 - r_{\rm S}/r} \left\{ \left[1 - \frac{b^2}{r^2}\left(1 - \frac{r_{\rm S}}{r}\right)\right]^{-1/2} - 1 \right\} \tag{42}$$

is the time difference between photons originating from the same radius (R) and

$$\delta t(r_{ref}, R) = R - r_{ref} + r_{\rm S} \ln(\frac{R - r_{\rm S}}{r_{ref} - r_{\rm S}}) \tag{43}$$

is the time difference between photons with $b = 0$ from R and r_{ref}.

In the case when $\alpha > \pi/2$ the corresponding delay is

$$\begin{aligned} c\Delta t(R,\alpha) &= 2c\Delta t_s(p,\pi/2) - c\Delta t_s(R,\pi-\alpha) \\ &+2\left[R - p + r_{\rm S}\ln(\frac{R - r_{\rm S}}{p - r_{\rm S}})\right] - \delta t(r_{ref}, R). \end{aligned} \tag{44}$$

For a given pulsar phase ϕ, we compute angle ψ, then we find the corresponding emitted α, σ and the impact parameter using formulae (27), (28) and (26), and compute the corresponding delays $\Delta t(R,\alpha)$ or $\Delta t_p(R,\alpha)$ with equations (41) and (44). We then construct a one-to-one correspondence between the pulsar phase ϕ and the photon arrival phase to the observer $\phi_{\rm obs} = \phi + \Delta\phi$, with the phase delays

$$\Delta\phi(\phi) = 2\pi\nu\Delta t[b(\phi)]. \tag{45}$$

The flux at observed phase $\phi_{\rm obs}$ is $F_{\rm obs}(\phi_{\rm obs}) = F(\phi_{\rm obs} - \Delta\phi)$ with phase delay $\Delta\phi = 2\pi\nu\Delta t$ computed using (41), (44) and (45). The effect of the photon arrival time contraction (or stretching) on the observed flux is already accounted for by one of the Doppler factors, so there is no need to multiply again flux by δ.

2.1.6 Profiles from a large spot

For a finite size spot, obviously, integration over the spot surface is required. The idea is to split the spot into a number of small sub-spots and compute the profiles from each sub-spot separately. One should be careful to include time delays correctly. (For this problem it is actually good to compute the time delays relative to the photons emitted from the point directly under the observer.) Integration over the spot surface is done using Gaussian quadrature in (cosine of) colatitude and trapezoidal rule for integration over the azimuth inside the spot. The surface element of the spot is

$$\mathrm{d}S(\theta) = R^2(\theta)[1 + f^2(\theta)]^{1/2} \sin\theta \mathrm{d}\theta \mathrm{d}\phi, \tag{46}$$

where the factor $[1 + f^2(\theta)]^{1/2}$ takes care of the oblateness of the spot surface (function $f(\theta)$ is given in equation 13).

Alternatively, one can use the HEALPIX representation of the spot, or any other routine. For a large spot (angular radius $\sim$30 deg), at least a few tens points in total are needed if one wants to achieve accuracy of the order of 1%.

2.1.7 Comparison of the profiles

2.2 Bayesian inference

The model presented in the previous section, can be used to constrain parameters of neutron stars by using Bayesian methods. We can fit observed data to the model and use Markov Chain Monte Carlo (MCMC) methods to sample over the parameter space and find the most probable values for the parameters of the model. The data can also be synthetic (as in this Thesis) in order to test if the sampler will actually find the same values that were used when creating the data. More about the synthetic data is presented in the Results section.

The aim of this work is to determine the most probable ("best-fit") values of the parameters in the pulse profile model, given the "observed"waveform, and the confidence regions for the values of these parameters. Probabilities are calculated using Bayes's theorem, which is presented in the next section. The standard Metropolis sampling method of the parameter space and a quite new ensemble sampler (used in this thesis) are discussed in the two following sections.

2.2.1 Bayesian analysis

We are interested in the probability distributions of the parameters $\mathbf{y}$ of the waveform model when the observed waveform is known. The probability is marked $p(\mathbf{y}|D)$, where D is the energy- and oscillation phase-resolved waveform data (synthetic in this Thesis). According to the Bayes's theorem this (posterior) probability distribution can be obtained from the likelihood of the data, given the parameter values:

$$p(\mathbf{y}|D) \propto p(D|\mathbf{y})p(\mathbf{y}). \tag{47}$$

In the previous equation $p(D|\mathbf{y})$ is the likelihood or the probability distribution of the data given the parameters. The next factor $p(\mathbf{y})$ is the prior probability distribution of the parameter values. As a first approximation we use uniform prior, which is the most uninformative prior. Later we take account the information of polarization measurements and make the priors of inclination and spot colatitude non-uniform to see how or if it is improving the fits. The constant of proportionality is the inverse of the normalization factor, but it is irrelevant when estimating the values of the parameters in a given model.

2.2.2 Metropolis (-Hastings?)

The original, standard MCMC algorithm is called the Metropolis algorithm. It is a MCMC method for obtaining a sequence of random samples from a probability distribution. It generates random samples by moving in a random walk; that is some sequence $X_1 ... X_t$. Metropolis algorithm, like all the other MCMC sampling methods, satisfy the so called Markov property. It means that the conditional distribution of X_{t+1} given all past elements is independent of all but the previous state:

$$P(X_{t+1} = x | X_t ... X_1) = P(X_{t+1} = x | X_t). \tag{48}$$

A Markov chain is a random walk with Markov property.

The Metropolis algorithm works by taking an arbitrary move near the current point. If X_t is the sample at time t, then the new sample Y is proposed from the proposal distribution $q(Y|X_t)$. The likelihood of this new sample is then compared to that of the previous sample. The likelihood ratio α between the to states is calculated with the following equation:

$$\alpha = \frac{p(Y|D)q(X_t|Y)}{p(X_t|D)q(Y|X_t)}. \tag{49}$$

The conditional probabilities given the data are calculated using the Bayesian formula (47). The ratio of these probabilities is multiplied with the ratio of proposal distributions (sometimes called transition kernels) so that the algorithm satisfy condition called detailed balance. It is an important property for proving the convergence of the chain. It states that a step from X_t must have the same probability as a step from Y to X_t. The proposal density $q(X_t|Y)$ describes the probability of a transition from Y j to X_t in the parameter space.

The next step is to decide whether the likelihood ratio is high enough in order to accept the new step. In Metropolis(-Hastings) algorithm, we automatically accept a step, if $\alpha \geq 1$, but otherwise with a probability α (if α is greater than a random number between 0 and 1). If the new state is accepted, we repeat the first steps using now Y as the current point. Otherwise we propose the new sample using again the same X_t.

It can be seen that the acceptance rule simplifies considerable when the proposal density is indeed symmetric ($q(X_t|Y)$=$q(Y|X_t)$). The algorithm is typically repeated until the obtained chains are long enough in the sense that their statistics do not change significantly when adding new members to the chain. Whether the obtained samples are statistically representative of the posterior can be verified if several chains with different initial states result in the same posterior density.

Metropolis algorithm has also some limitations. The generated samples are not independent, since they are generated in a chain (concerns also other MCMC methods). The correlation between the samples can be measured by the autocorrelation time (ADD DEFINITION...and more).

One major disadvantage is that the Metropolis algorithm may work poorly for skewed, or anisotropic, distributions, depending on the proposal distribution (ADD EXAMPLES). Partially for this reason we have moved to use the ensemble sampler, which is presented in the next section.

2.2.3 Ensemble sampler

The affine invariant ensemble sampler is a novel MCMC method developed a few years ago (Goodman, Weare...). The algorithm has a similar structure to Metropolis, and still uses a proposal and and accept/reject step. But instead of only one sequence $X_1 ... X_t$, we use now a group or ensemble of sequences. Each member of the ensemble is called a walker. On each iteration the algorithm generates a new sample for every walker using the current positions of all of the other walkers in the ensemble. However each walker is independent of the other walkers and is not correlated with the previous states of other walkers (it is correlated only to its own previous state).

The ensemble sampler is called affine invariant, since its performance is unaffected by affine transformations of space. This means that sampling a PDF g(x) = Af(x) + b is equivalent to sampling f then applying A and b after. This is the reason why the algorithm is particularly useful for sampling badly scaled distributions. Computational tests show that the affine invariant methods can be significantly faster than standard MCMC methods on highly skewed distributions.

In ensemble sampler the Markov chain is evolved by moving one walker at time. Each walker X_k is updated using the current positions of all of the other walkers in the ensemble (we call them complementary ensemble). The motivation is that the distribution of the walkers in the complementary ensemble carries useful information about the probability density of the parameters. This way the trial move can be adapted to the target density.

One of the simplest affine invariant trial moves is stretch-move (we use it). In a stretch-move each walker is moved using only one randomly selected complementary walker (see Fig. 2). The move proposed alone a line between the current walker k and the complementary walker j according to the distribution

$$Y = X(j) + Z(X(k) - X(j)), \tag{50}$$

where the scaling variable Z satisfy the symmetry condition

$$g(1/z) = zg(z). \tag{51}$$

This ensures that the move 50 is symmetric in the usual informal way Metropolis is discussed (detailed balance is satisfied).

When deciding whether the new sample is good enough, the Metropolis-Hastings selection rules are again applied. However instead of equation 49 the likelihood ratio is now

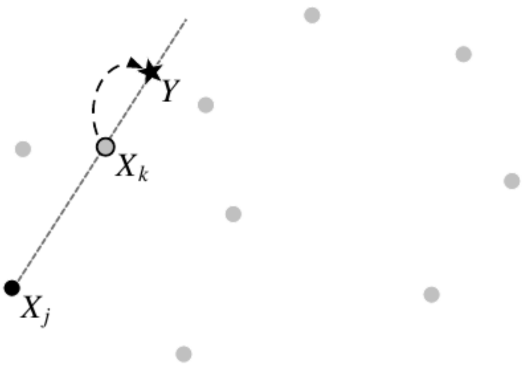

Fig. 2. A stretch move for updating the position of X_k based on the position of another random walker, X_j (subscript identifies here the walker instead of the step count). The light-gray walkers are other members of the ensemble. Figure 2 from Goodman and Weare (2010).

calculated (for a given walker)

$$\alpha = Z^{N-1}\frac{p(Y|D)}{p(X_t|D)}, \tag{52}$$

where N is the number of parameters sampled.

2.2.4 Implementation

3 Results

3.1 Synthetic data

3.2 Parameter constraints

4 Summary and Conclusions

References

[1] J. M. Lattimer and M. Prakash, Science 304:536-542,2004 (2004).

[2] C. Rhoades and R. Ruffini, Phys. Rev. Lett. 32, 324 (1974).

[3] A. Patruno and A. L. Watts, ArXiv e-prints (2012).

[4] M. Gierli´nski, C. Done and D. Barret, MNRAS 331, 141 (2002).

[5] J. Poutanen and M. Gierlinski, MNRAS 343, 1301 (2003).

[6] K. R. Pechenick, C. Ftaclas and J. M. Cohen, APJ, 274, 846-857 (1983).

[7] M. AlGendy and S. M. Morsink, Universality of the Acceleration Due to Gravity on the Surface of a Rapidly Rotating Neutron Star, 2014.

[8] S. M. Morsink, D. A. Leahy, C. Cadeau and J. Braga, Astrophys.J.663:1244-1251,2007 (2007).

[9] C. Misner, K. Thorne and J. Wheeler, *Gravitation* (W. Freeman, 1973), .